Effect of bending instabilities on the measurements of mechanical properties of multiwalled carbon nanotubes

Jefferson Z. Liu,[1] Quanshui Zheng,[1,*] and Qing Jiang[2,†]
[1]*Department of Engineering Mechanics, Tsinghua University, Beijing 100084, China*
[2]*Department of Mechanical Engineering, University of California, Riverside, California 92521*
(Received 1 July 2002; revised manuscript received 4 October 2002; published 26 February 2003)

It has been reported that a multiwalled carbon nanotube in bending may exhibit an unusal elastic mode that corresponds to the wavelike distortion or ripple along the inner arc of the bent nanotube, called the rippling mode, which cannot be predicted by the linear theories. The present analysis shows that the rippling mode is permissible by the theory for highly anisotropic elastic materials of finite deformation and that the dependence of the bending moment upon the bending curvature can be well approximated by a bilinear relation, in which the transition from one linear branch to the other corresponds to the emergence of the rippling mode. With this bilinear relation, the authors show that the deflection response to a transverse force is consistent with the unusual behavior reported by Wong, Sheehan, and Liebert [Science **277**, 1971 (1997)]. Furthermore, their analysis indicates that there exists a critical diameter, for given load and length, which corresponds to the emergence of rippling mode, and that the effective Young's modulus of multiwalled carbon nanotubes at the vibration resonance drops sharply as the diameter increases to surpass this critical value, confirming a phenomenon observed by Poncharal, Wang, Ugarte, and de Heer [Science **283**, 1513 (1999)].

DOI: 10.1103/PhysRevB.67.075414 PACS number(s): 62.25.+g, 62.30.+d

INTRODUCTION

Carbon nanotubes have been recognized as important nanoscopic systems since their discovery in 1991,[1] and hold the promise of a variety of applications because of their unique molecular structure and their fascinating mechanical and electronic properties. For instance, carbon nanotubes have been expected to be the ultimate fibers because of the theoretical predictions, such as Robertson *et al.*,[2] Calvert,[3] Overney *et al.*,[4] Yakobson *et al.*,[5] and Krishnan *et al.*,[6] that their axial strength is extremely high and that their elastic modulus along the tube axis is as large as the Young's modulus along the basal plane of highly oriented pyrolythic graphite, which is on the order of one terepascal (TPa). Carbon nanotubes have hence been under continuous investigation for applications as constituents in composite materials[7] and also as components of nanoscale instruments, such as probes of high-resolution scanning force microscopes,[8] nanobearings of super low friction,[9] and molecular oscillators of frequency as high as several gigahertz.[10,11] These have led to many investigations on determination of the mechanical properties of carbon nanotubes, the axial Young's modulus in particular. For example, Treacy *et al.*[12] measured the amplitudes of intrinsic thermal vibration of cantilevered carbon multiwalled nanotubes (MWNT) using the transmission electron microscopy, and this leads to the energy associated with each of the vibration modes by assuming equipartition among all the vibration modes. By further postulating that the probability of a sample nanotube taking a vibration mode obeys the Gaussian distribution and by assuming that the Young's modulus-frequency relation for each mode predicted by the linear vibration analysis of cantilevered beams remains valid, they estimated that the axial Young's modulus E varied from 0.4 to 3.7 TPa, with a mean value at 1.8 TPa. Wong *et al.*[13] measured the dependence of deflection of a cantilevered multiwalled carbon nanotube upon an external force applied at different locations along the nanotube, using the atomic force microscopy (AFM), and they then obtained the axial Young's modulus E of $1.28+$ or -0.59 TPa by fitting their data with a force-deflection relation resulting from the linear analysis of cantilevered beams. Using the transmission electron microscopy, Salvetat[14] measured the variation of deflection of a suspended multiwalled carbon nanotube spanning over a hole in response to a force acting at the middle point of the nanotube, and they obtained the axial Young's modulus E in the range of $0.65\sim1.22$ TPa, using a force-deflection relation of the linear theory for simply supported beams. Poncharal *et al.*[15] measured the fundamental resonance frequency of multiwalled carbon nanotubes induced by an alternating electric field in a transmission electron microscope and they then calculated the axial elastic modulus using the following modulus-frequency relation resulting from the classical analysis of linear elasticity for cantilevered beams:[16]

$$\Omega_n=\frac{\omega_n^2}{L^2}\sqrt{\frac{EI}{\rho A}}, \tag{1}$$

where L, A, I, and ρ are, respectively, the length, the cross sectional area, the moment of inertia of the cross section, and the mass density per unit length of the beam. Here Ω_n, $n=0,1,2,\ldots,$ are the resonance frequencies and ω_n are the roots of the equation $\cos\omega_n\cosh\omega_n+1=0$, each of which corresponds to a vibration mode of the cantilevered beam, being viewed as a normalized resonance frequency. For instance, $\omega_0\approx1.875$, corresponds to the fundamental mode of vibration. Poncharal *et al.*[15] reported that their so-determined E decreases sharply from about 1 to 0.1 TPa with the tube diameter increasing from 8 to 40 nm. To their credit, Poncharal *et al.* have cautioned the readers by calling E the elastic bending modulus, instead of the Young's modulus. Yu *et al.*[17] performed a tensile test by attaching two ends of an

individual multiwalled nanotube onto the opposing tips of two AFM probes, which are operated inside a scanning electron microscope (SEM) and which act as both the force sensor and the displacement sensor. In order to determine the Young's modulus, they need to calculate the strain and the stress, commonly defined as the elongation per unit length and the force per unit loading area, respectively, but they could not determine the effective loading area because how the load was shared by the individual walls of this multiwalled nanotube is not entirely clear. They estimated the upper limit of the Young's modulus varying from 270 to 950 GPa by assuming that only the outermost wall was subjected to the load, and the lower limit varying from 18 to 68 GPa by assuming that the load is uniformly distributed over the cross-sectional area of each of the walls. Yu *et al.*[18] later applied the same technique to load the ropes of single-walled carbon nanotubes, but they again could not determine the actual loading area because the nanotubes in the loaded rope did not share the tensile load equally.

We note that Yu and co-workers[17,18] treated a nanotube as a homogenous continuum tube whose thickness is the representative thickness of the graphite interplanar spacing (0.34 nm), for a single-walled, and is the difference in the outer and inner radius, for a multiwalled, as many other investigators did. Yakobson *et al.*[19] have shown that the linear and isotropic elastic shell model of continuum theory, with a few properly chosen parameters, can predict deformations of carbon nanotubes remarkably well, and they have compared the continuum shell model with the detailed *ab initio* and semiempirical studies of single-walled carbon nanotubes. Their comparison[19] shows that the flexural rigidity given by the continuum shell model is substantially larger than that predicted by the atomistic studies, if the wall thickness and the Young's modulus of the shell are, respectively, taken to be the representative thickness of the graphite interplanar spacing (0.34 nm) and the in-plane elastic modulus of graphite (1.06 TPa). To make the continuum shell model equivalent to the atomistic model for calculating deformations, they[19] have suggested that the representative thickness of the continuum shell be taken as 0.066 nm, and correspondingly, this leads to the Young's modulus of the continuum shell as large as 5.5 TPa. They have further shown that the classic results of the continuum shell model can readily predict the mechanical behavior of single-walled carbon nanotubes, including axial compression, bending, and torsion, with the so-chosen numerical values for the wall thickness and the Young's modulus. Ru[20] has later raised his concerns that a set of concentric Yakobson's equivalent shells, each modeling a wall of a multiwalled carbon nanotubes, would have interior gaps between adjacent shells of interwall spacing of 0.34 nm, leading to some inconvenience in application of the results from the classic continuum shell model to multiwalled carbon nanotubes. He[20] has hence proposed that the flexural rigidity of the equivalent continuum shell, modeling a single-walled carbon nanotube, should be regarded as an independent material parameter, instead of a parameter derivable from the representative wall thickness, Young's modulus and the Poisson ratio, as given in a classic result from the linear and isotropic elastic continuum shell model, and this would permit him to set the thickness of the equivalent shell be the representative thickness of the graphite interplanar spacing (0.34 nm) and to model a multiwalled carbon nanotubes as a set of concentric equivalent shells with no interior gaps between adjacent shells. In the present study, we treat a multiwalled carbon nanotube as a homogeneous continuum beam whose representative thickness is taken to be the difference in the outer and inner radius.

We should point out that all of these experimental measurements are indirect primarily because the difficulties associated with handling such samples of extremely small diameters have prevented the researchers from obtaining reliable values through direct measurements, and we further note that all the estimates of the elastic modulus cited above rely on the results of the linear theories for bending deformation and/or bending vibrations of elastic beams, except the works of Yu *et al.*,[17,18] which have led to their estimated upper and lower limits of the Young's modulus, instead of the modulus itself. There, however, are evidences that the behavior of the carbon nanotubes in some of these experiments is not entirely linear, though elastic essentially. For instance, Poncharal *et al.*[15] have observed the another bending mode for thick multiwalled carbon nanotubes that corresponds to the wavelike distortion or ripple on the inner arc of the bent nanotube, and they have suggested that the sharp decrease in their reported bending modulus may be attributable to the emergence of the rippling mode in bending. A similar explanation was offered (without details) by Yakobson and Avouris.[19] Liu *et al.*[21] have recently presented a perturbation analysis based on the nonlinear vibration theory, which shows that the effective bending modulus, not the actual axial Young's modulus, drops substantially with the increasing tube diameter due to the emergence of the rippling bending mode. We note that the rippling bending mode was previously observed by Ruoff and Lorents,[22] Kuzumaki *et al.*,[23] and Wong *et al.*[13] for multiwalled carbon nanotubes. Wong *et al.*[13] have noted the abrupt decrease of the initial constant slope in the force-deflection bending curve at a relatively large deflection of their multiwalled carbon nanotubes, and they have also noted the subsequent increase of the stored strain energy with the further deflection at a significantly slower rate. Prior to this point, the strain energy increases quadratically with the strain as expected for a harmonic system, indicating that the deflection response to the external force is linear prior to this point. Wong *et al.*[13] suspected that this was due to the elastic buckling, a phenomenon previously observed by Iijima *et al.*[24] for multiwalled carbon nanotubes using a high resolution transmission electron microscope. Here we note the excellent agreement between the measured bending strength by Wong *et al.*[13] and the predicted values by Smalley and Yakobson[25] using the equivalent continuum shell model. Smalley and Yakobson explained that the bending strength measured by Wong and his colleagues was determined by the layer delamination of the multiwalled nanotube on the compression side, and they modeled the delamination event as buckling of an elastically supported plate. There have also been many computer simulations of buckling of carbon nanotubes using different empirical atomic interaction potentials, such as Refs. 5,26, and

27, but most of these simulations are limited to single-walled carbon nanotubes with few exemptions, such as the work of Iijima *et al.*[24] and the work of Garg and Sinnott.[28] This is primarily due to the fact that computer simulations of multiwalled carbon nanotubes remain prohibitively expensive. With a detailed comparison of their observations with the simulations, Wong *et al.*[13] have noticed the characteristic difference between the observed bending behavior and the simulation results. The simulations predict that the external force drops about 30% at buckling and it remains nearly constant during further deflection. However, the measurements of Wong *et al.* show an insignificant decrease in force at the perceived buckling point and the continuing increase of the force, though at a slower rate, during further deflection. Also, the stored strain energy increased nonlinearly with further deflection beyond the perceived buckling point, instead of linearly as the computer simulations predicted. This has brought the question whether the multiwalled carbon nanotubes had buckled in the experiment, or had switched at this point from one bending mode to another.

According to the elastic (not necessarily linear) beam theory, the bending moment $M(x,t)$ and the beam deflection $w(x,t)$ at each time instant t are related by the following equation:[16]

$$M'' + \rho A \ddot{w} = F, \tag{2}$$

where $F(x,t)$ denotes the applied load measured per unit length, and w' and $\dot{w}$ the partial derivatives $\partial w(x,t)/\partial x$ and $\partial w(x,t)/\partial t$, respectively. M is constitutively related to the bending curvature κ, which is associated with the deflection w in the form $\kappa = w''/[1+(w')^2]^{3/2}$ and is approximated by w'' for cantilevered beams that involve no conspicuous rotations. For small bending deformations, a linear constitutive relation provides a fairly good approximation, and the linear theory of elasticity leads to $M = EIw''$. With this linear constitutive relation, Eq. (2) leads to the resonance frequencies given by Eq. (1) for cantilevered beams. Considering that the linear theory cannot lead to the emergence of the rippling mode, we are interested in the nonlinear effect of the constitutive relation on the bending behavior. Our numerical analysis based on the theory of finite elasticity suggests that the rippling bending mode is permissible by the nonlinear theory and that the dependence of the bending moment upon the bending curvature can be well approximated by a bilinear relation, in which the transition from one linear branch to the other corresponds to the emergence of the rippling bending mode. With this bilinear constitutive relation, we study the mechanical properties of our model nanotubes, respectively, under static deflection as that in the experiment of Wong *et al.*[13] and at the vibration resonance as that in the experiment of Poncharal *et al.*[15] Our analysis shows that the mechanical response both in the external load and in the stored strain energy versus the deflection, of our cantilevered model nanotube in the rippling bending mode is consistent with the observation of Wong *et al.*[13] Also, the analysis on the resonance vibration indicates that the effective bending modulus, instead of the actual Young's modulus, suffers a sharp drop as the rippling bending mode emerges. This suggests that one need to be particular cautious in using the classical results from the linear elasticity to derive the mechanical properties of carbon nanotubes from measurements, because their responses to probing are not always linear, and that the rippling bending mode appears to be responsible for the unusual mechanical behaviors in bending deflection reported by Wong *et al.*[13] and in resonant vibration reported by Poncharal *et al.*[15]

I. APPROXIMATED BILINEAR CONSTITUTIVE RELATION

In principle, to obtain the nonlinear bending moment/curvature relation, we should conduct a full-scale nonlinear analysis for a model nanotube subjected to pure bending (i.e., the bending moment is the sole resultant load throughout the beam), using the three-dimensional theory of finite elasticity. This task proves to be overwhelmingly complex to us because of the locally large deformation, uncertainty of rippling period, and the strong material anisotropy of multiwalled carbon nanotubes. For simplicity, we consider a graphite nanobeam of a rectangular cross-section bent in a plane, and we assume that the graphite base plane of this nanobeam is parallel to the beam axis and perpendicular to bending plane. We note that the linear constitutive relation for graphite is well documented.[29] It is, however, unfortunate that the elastic moduli of the second-order and higher for graphitic carbon are unavailable in the literature.[29] Because of our interest in the nonlinear effect, we constructed an approximated constitutive relation, with the available linear elastic moduli,[29,30] by replacing the infinitesimal strain tensor commonly used in the linear theory with the Green strain tensor of the finite deformation theory.[31]

As reported in our previous work,[21] we conducted a numerical analysis for such a model nanobeam subjected to pure bending, using a commercial finite element code ABAQUS and with considerable efforts directed to search a rippling configuration. We note that the extremely small rippling period, a fraction of the model beam height (the nanotube diameter), makes our iterative procedure for searching the rippling configuration impractically expensive for a model beam of a length/height ratio as large as those of the sample nanotubes used in the experiment.[15] Fortunately, it is theoretically known that the bending moment is independent of the length/height ratio for beams of the linear constitutive relation and subjected to pure bending, provided that the length is an integer multiple of the rippling period. In this analysis, we assume that our model nanobeam is subjected to the so-called plane stress condition, i.e., all the nonzero components of the stress tensor are within the bending plane. Considering that the rippling period is not a predeterminable parameter and the rippling configuration may exhibit certain degree of sensitivity to the choice of finite element meshes, we have carried out finite element analyses for beams with a number of different combinations of the length/height ratio and the mesh number along the beam height, as shown in Table I.

The four node quad mesh was used and the calculation steps are automatically controlled by ABAQUS. This analysis

TABLE I. Combinations of the length/height ratio and the mesh number along the beam height used in the ABAQUS simulations of rippling configurations in the work of Ref. 21.

Length/height ratio	15	20	10	12	15	18	20
Mesh number along the beam height	8	8	12	12	12	12	12

confirms that the model nanobeam does experience a transition from the classical bending mode predicted by the linear theory to a rippling bending mode under severe bending. Figure 1 shows a typical rippling configuration for such a beam with the length/height ratio $L/d=10$ and the mesh number 8 along the beam height. It is seen that the rippling period is about one fourth of the beam height d, consistent with the experimental observation of Poncharal *et al.*,[15] although the rippling configurations are slightly dependent on the length/height ratio as well as the finite element meshes. With the numerical results, we have calculated the bending curvature and the corresponding bending moment, and we have plotted in Fig. 2 the normalized bending moment $\bar{M} \equiv Md/(2EI)$ versus the normalized bending curvature $\bar{\kappa} \equiv \kappa d/2$ at each loading step for our model beams of length/height ratios 10,15,20. Here, d denotes the beam height or the tube diameter in the later discussion, and $\bar{\kappa}$ is actually the maximum strain over the cross-section area.

We note from Fig. 2 that the numerical data for the bending moment versus the bending curvature can be well fitted with the following bilinear relation:

$$\bar{M}(\bar{\kappa})=\begin{cases} \bar{\kappa} & \text{if } 0\leqslant\bar{\kappa}<\bar{\kappa}_{\rm cr}, \\ \bar{\kappa}_{\rm cr}+\alpha(\bar{\kappa}-\bar{\kappa}_{\rm cr}) & \text{if } \bar{\kappa}\geqslant\bar{\kappa}_{\rm cr}, \end{cases} \tag{3}$$

where the dimensionless transition curvature $\bar{\kappa}_{\rm cr}$ is about 0.006, at which the beam switches from the classical bending mode to the rippling bending mode, and the dimensionless parameter α is about 0.19, which characterizes the increase of the dimensionless bending moment with further deflection. We note that the normalized bending moment $\bar{M}(\bar{\kappa})$ is an odd function of the normalized bending curvature $\bar{\kappa}$. For multiwalled carbon nanotubes of very small inner diameters, our numerical analysis[32] shows that the bilinear constitutive relation (3) severs as a good approximation, with a larger $\bar{\kappa}_{\rm cr}$ and a slightly larger α. We turn now to examine the implications of this approximated bilinear constitutive relation on the characteristics of our model nanotube under static deflection and at vibration resonance, respectively, in the following two sections.

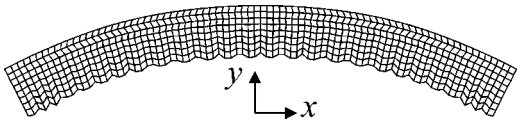

FIG. 1. Rippling of a nanobeam under pure bending simulated with ABAQUS using the four-node quad mesh (after Ref. 21). The length/height ratio is 10 and the mesh number in the height direction is 8.

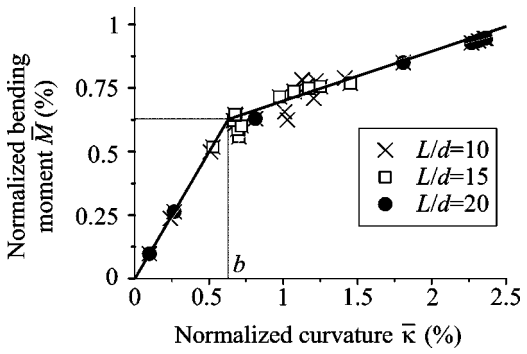

FIG. 2. The normalized bending moment-curvature relation resulting from the numerical analysis (discrete points) and the bilinear approximation (solid lines).

II. EFFECT OF THE RIPPLING MODE ON STATIC DEFLECTION

We now consider a multiwalled carbon nanotube cantilevered at one end and subjected to a lateral force P at the other end, and we are interested in the deflection at the loading point, called the displacement, both before and after the emergence of the rippling bending mode. With the x axis pointing from the cantilevered end ($x=0$) to the loaded end ($x=L$), the bending moment caused by the load P is given as $M(x)=P(L-x)$, as yielded from the static version of Eq. (2). The corresponding curvature $\kappa(x)$ must monotonically decrease with the axial coordinate x, because of the monotonicity of the bending moment. We denote the point that divides the nanotube into two portions by $x=L_{\rm cr}$: one portion in the rippling bending mode ($0<x<L_{\rm cr}$) and the other portion in the classical bending mode ($L_{\rm cr}<x<L$), and correspondingly, we have $\bar{\kappa}(L_{\rm cr})=\bar{\kappa}_{\rm cr}$. Thus, the constitutive relation (3) leads to

$$L-L_{\rm cr}=\frac{2EI\bar{\kappa}_{\rm cr}}{Pd}=\frac{EI\kappa_{\rm cr}}{P}, \tag{4}$$

where $\kappa_{\rm cr}=2\bar{\kappa}_{\rm cr}/d$ is the critical curvature. Requiring $L_{\rm cr}>0$ leads to

$$P>P_{\rm cr}\equiv\frac{2EI\bar{\kappa}_{\rm cr}}{Ld}=\frac{EI\kappa_{\rm cr}}{L}, \tag{5}$$

where the critical load $P_{\rm cr}$ is the minimum force required for the rippling bending mode to emerge from the cantilevered end where the bending is most severe. Combining Eq. (4) with Eq. (5) yields

$$1-\frac{L_{\rm cr}}{L}=\frac{P_{\rm cr}}{P}. \tag{6}$$

If $P<P_{\rm cr}$, the entire nanotube is in the classical bending mode and thus we have from the constitutive relation (3):

$$\frac{P(L-x)}{EI}=\kappa(x) \quad \text{for } 0<x<L. \tag{7}$$

Approximating the curvature by the second spatial derivative of the deflection function $w(x)$ and integrating the resulting differential equation lead to the classical solution for the displacement (i.e., the deflection at the loading point):

$$\Delta = \Delta_0 \equiv \frac{PL^3}{3EI}, \quad \text{for } P < P_{\rm cr}. \tag{8}$$

In the case that $P > P_{\rm cr}$, the constitutive relation (3) leads to

$$\begin{cases} \dfrac{P(L-x)}{EI} = (1-\alpha)\kappa_{\rm cr} + \alpha w''(x) & \text{for } 0 < x < L_{\rm cr}, \\ \dfrac{P(L-x)}{EI} = w''(x) & \text{for } L_{\rm cr} < x < L. \end{cases} \tag{9}$$

We then solve Eq. (9) with the cantilevered boundary conditions $w(0) = w'(0) = 0$. We require that the deflection function $w(x)$ and its first derivative $w'(x)$ be both continuous at the transition point $L_{\rm cr}$, and we note that this is in contrary to buckling where the derivative of the deflection function suffers a finite jump. This requirement leads to the following expression for the displacement:

$$\Delta = \Delta_0 \left[1 + 3\beta \left(1 - a^2 + \frac{1}{3}a^2 \right) a - 3\beta \frac{P_{\rm cr}}{P} \left(1 - \frac{1}{2}a \right) a \right] \quad \text{for } P > P_{\rm cr}, \tag{10}$$

where $a = L_{\rm cr}/L$ and $\beta = (1-\alpha)/\alpha$. We now introduce the normalized displacement and the normalized load

$$\delta = \frac{\Delta}{\Delta_{\rm cr}}, \quad p = \frac{P}{P_{\rm cr}},$$

where $\Delta_{\rm cr} = P_{\rm cr} L^3/(3EI)$ is the displacement corresponding to the critical load $P_{\rm cr}$. Substituting Eq. (6) into Eq. (10) yields

$$\delta = p + \beta \left(\frac{7}{2} + p \right) \left(1 - \frac{1}{p} \right)^2 \quad \text{for } P > P_{\rm cr}. \tag{11}$$

We turn now to calculate the stored strain energy, which should be equal to the work done by the external force because the deformation appears to be elastic, as reported[13] and thus the stored strain energy is given below:

$$U = \int_0^{\Delta} \hat{P}(\Delta) d\Delta = P\Delta - \int_0^{P_{\rm cr}} \frac{PL^3}{3EI} dP - \int_{P_{\rm cr}}^{P} \hat{\Delta}(P) dP, \tag{12}$$

where the loading-deflection relation $P = \hat{P}(\Delta)$ or equivalently $\Delta = \hat{\Delta}(P)$ is defined implicitly by Eq. (10). Substituting Eq. (10) into Eq. (12) and using Eq. (8) yields

$$U = \begin{cases} U_0 \quad \text{for } P \leqslant P_{\rm cr}, \\ U_0 \left[1 + \beta \left(1 - 3\dfrac{P_{\rm cr}^2}{P^2} + 2\dfrac{P_{\rm cr}^3}{P^3} \right] \right. \quad \text{for } P > P_{\rm cr}, \end{cases} \tag{13}$$

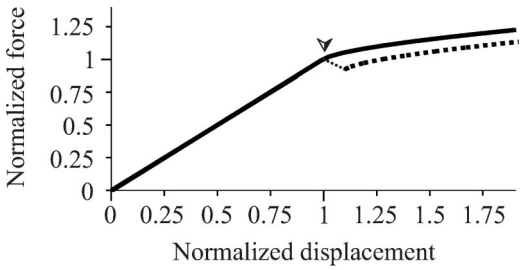

FIG. 3. The normalized lateral force versus the normalized displacement. The dotted line accounts for the kinking effect at the transition point.

where $U_0 = P^2 L^3/(6EI)$ is the stored strain energy in the classical bending mode.

We recall the experiment of Wong *et al.*[13] where they pushed a multiwalled carbon nanotube by the tip of an AFM probe, and they recorded the pushing force versus the controlled displacement of the AFM probe. For a qualitative comparison, we have plotted in Fig. 3, with $\alpha = 0.19$, the normalized load $p = P/P_{\rm cr}$ versus the normalized deflection $\delta = \Delta/\Delta_{\rm cr}$ (the solid curve). We note in Fig. 3 the abrupt decrease of the initial constant slope in the force-displacement plot at $p = 1$ (i.e., $P = P_{\rm cr}$) where the rippling mode emerges. We note from Eq. (13) that the stored strain energy increases with the further deflection nonlinearly after the emergence of the rippling, being contrary to the linear increase of the stored strain energy in post-buckling as predicted by the computer simulations.[5,24,26,27] It is seen from Eq. (13) that the stored strain energy increases quadratically prior to this point, and departs, at this point, from the response expected for a harmonic system, resulting in the subsequent increase of the stored strain energy with the further deflection at a significantly slower rate. All the above features are consistent with what Wong *et al.*[13] reported except the absence of a small drop in the loading force at the transition point, which was indicated by the measurements of Wong *et al.*[13] This may be qualitatively explained by considering the elastic effect of the cantilevered AFM probe.[34] We also note that the classic bending mode and the rippling bending mode are, probably, both locally metastable when the bending curvature is approximately equal to the critical curvature and correspondingly, there is a small energy barrier to be overcome for the transition from the classic bending mode to the rippling bending mode to take place. The physical mechanism of this transition is beyond the scope of this discussion, although one may model the macroscopic behavior corresponding to the transition using a phenomenological approach by introducing an empirical or semi-empirical kinetic relation. In summary, the above analysis indicates that the abrupt change in the deflection response of the carbon nanotubes to the AFM probing reported by Wong *et al.*[13] appears to correspond to the emergence of the rippling bending mode, instead of buckling as perceived by those investigators who, nevertheless, should be credited for their caution that the characteristics of the measured response are somewhat different from those of post buckling as predicted by the computer simulations.

III. EFFECT OF THE RIPPLING MODE ON RESONANCE

To study the resonance behavior, we recall the experiment of Poncharal *et al.*,[15] in which the sample multiwalled carbon nanotubes were precharged statically with a biasing voltage $V_s = 20$ V before they were driven to vibrating by a harmonic oscillating voltage of magnitude $V_d \approx 0.1$ V, superimposed upon the static voltage. These correspond to two forces acting at the free end of the carbon nanotube, a static force P_s and a time-harmonic force $P_d \cos(\Omega t)$, and each induced force equals the product of the induced electric charge (proportional to the voltage) and the electric field (also proportional to the voltage), as Poncharal *et al.*[15] pointed out. Therefore, the force magnitude ratio P_d/P_s is proportional to the square of the voltage ratio $(V_d/V_s)^2 \approx 2.5\times 10^{-7}$. Considering that this force ratio is extremely small, we assume that if the rippling bending mode had emerged in a sample nanotube, it had occurred during the static loading prior to the dynamic loading. Thus, in the case that $P_s < P_{\rm cr}$, there is no rippling and hence the bending moment is proportional to the bending curvature as given in the first portion of the constitutive equation (3). Correspondingly, the governing equation (2) yields the classical result for the resonance frequency given by Eq. (1).

In the following, we are primarily interested in the fundamental resonance frequency of the model nanotube in the case that a portion of the nanotube ($0 < x < L_{\rm cr}$) had taken the rippling bending mode prior to the dynamic loading, and thus we assume $P_s > P_{\rm cr}$. We now study the resonance behavior of the preloaded model nanotube in response to the small harmonic loading $P_d \cos(\Omega t)$. Substituting the constitutive equation (3) into the governing equation (2) yields the following:

$$P_d \cos(\Omega t)\,\delta(L-x) - \rho A \ddot{w}(x,t) = \begin{cases} EI\alpha\kappa''(x,t) & \text{for } 0<x<L_{\rm cr}(t), \\ EI\kappa''(x,t) & \text{for } L_{\rm cr}(t)<x<L, \end{cases} \tag{14}$$

where $\delta(x)$ denotes the Dirac delta function. It is generally possible that the dynamic loading causes the length $L_{\rm cr}$ of the rippling portion to vary slightly with time, and this would make the analysis substantially more complicated. We assume that this variation is insignificant because the magnitude of the dynamic loading is extremely small in comparison with the static loading, and hence we neglect this variation for the benefit of the dramatic simplification of the present analysis. To determine the fundamental resonance frequency, we then turn to study the characteristics of the free vibration of such a partially rippled nanotube by setting $w(x,t) = LW(u)\cos(\Omega t)$, with $u = x/L$, and by noting that the deflection and its derivative both vanish at the cantilevered end and by requiring that there be neither a bending moment nor a shear force at the far end (free vibration), we have

$$W''''(u) - \varpi^4 W(u) = 0 \text{ for } 0<u<a \text{ and } W(0) = W'(0) = 0,$$
$$V''''(v) - \omega^4 V(v) = 0 \text{ for } 0<v<b \text{ and } V''(0) = V'''(0) = 0, \tag{15}$$

where

$$\omega = L\sqrt[4]{\frac{\Omega^2 \rho A}{EI}}, \quad \varpi = \frac{\omega}{\sqrt[4]{\alpha}}, \tag{16}$$

and the rescaling $v = 1-u$ and the deflection function $V(v) = W(1-u)$ for $a<u<1$ or $0<v<1-a=b$. The general solution of Eq. (15) is given by the following linear combinations of the harmonic and hyperbolic functions:

$$W(u) = C_1(\cos\varpi u - \cosh\varpi u) + C_2(\sin\varpi u - \sinh\varpi u) \text{ for } 0<u<a,$$
$$V(v) = C_3(\cos\omega v + \cosh\omega v) + C_4(\sin\omega v + \sinh\omega v) \text{ for } 0<v<b. \tag{17}$$

Furthermore, the deflection function, the bending moment and the shear force should all be continuous across the dividing point. In the case of our present interest where buckling does not occur, the deflection must be smooth at the dividing point. This leads to

$$W(a) = V(b), \quad W'(a) = -V'(b),$$
$$(1-\alpha)\kappa_{\rm cr} L + \alpha W''(a) = V''(b), \quad \alpha W'''(a) = -V'''(b). \tag{18}$$

Substituting Eq. (17) into Eq. (18) yields a system of four linear algebraic equations for the unknown constants C_1, C_2, C_3, and C_4, whose coefficient matrix depends upon the dimensionless excitation frequency ω. This coefficient matrix becomes singular as the dimensionless excitation frequency ω approaches one of the dimensionless resonant frequencies. Requiring the determinant of the coefficient matrix vanish leads to the following frequency equation:

$$\begin{aligned} 0 = {} & \alpha^{1/2}(1+\cos\varpi a\cosh\varpi a)(1+\cos\omega b\cosh\omega b) \\ & + \alpha^{-1/2}(1-\cos\varpi a\cosh\varpi a)(1-\cos\omega b\cosh\omega b) \\ & - \alpha^{1/4}(\cosh\varpi a\sin\varpi a - \sinh\varpi a\cos\varpi a) \\ & \times(\sinh\omega b\cos\omega b + \cosh\omega b\sin\omega b) \\ & - \alpha^{-1/4}(\cosh\varpi a\sin\varpi a + \sinh\varpi a\cos\varpi a) \\ & \times(\cosh\omega b\sin\omega b - \sinh\omega b\cos\omega b) \\ & - 2\sin\varpi a\sinh\varpi a\sin\omega b\sinh\omega b. \end{aligned} \tag{19}$$

The lowest root ω_R of the frequency equation corresponds to the fundamental resonance frequency $\Omega_R = (\omega_R^2/L^2)\sqrt{EI/\rho A}$, noting the definition (16) of the dimensionless excitation frequency. The effective Young's modulus $E_{\rm eff}$ is defined through the following equation:

$$\Omega_R = \frac{\omega_0^2}{L^2}\sqrt{\frac{E_{\rm eff} I}{\rho A}} \tag{20}$$

and this leads to

$$\frac{E_{\rm eff}}{E} = \left(\frac{\omega_R}{\omega_0}\right)^4. \tag{21}$$

We note, with significant interest, that the modulus-frequency relation (20) is formally identical to the classical relation (1), except that the effective Young's modulus E_{eff} has replaced the actual material Young's modulus E.

With Eq. (19) and the relations (16) and $b=1-a$, we note the dependence of the dimensionless fundamental resonance frequency ω_R upon the normalized rippling length $a=L_{\text{cr}}/L$ as well as the parameter α, and we thus denote it as $\omega_R(a,\alpha)$. As expected, our calculation shows that ω_R has the constant value $\omega_R(0,\alpha)=\omega_0\approx 1.875$ in the absence of rippling, as obtained from the linear theory, and $\omega_R(a,\alpha)$ and hence E_{eff} decrease with the increasing normalized rippling length a and the decreasing parameter α. Noting that $\overline{\kappa}=\overline{\kappa}_{\text{cr}}$ at $x=L_{\text{cr}}$, we obtain from Eqs. (10) and (4)

$$a\equiv\frac{L_{\text{cr}}}{L}=\begin{cases}0 \quad \text{for} \quad P<P_{\text{cr}},\\ 1-\dfrac{2\overline{\kappa}_{\text{cr}}L^2}{3\Delta_0 d} \quad \text{for} \quad P>P_{\text{cr}}.\end{cases} \tag{22}$$

Therefore, we conclude that the normalized rippling length a increases, and hence the effective Young's modulus E_{eff} decreases, with the increasing Δ_0, the increasing diameter d, and the decreasing length L, all monotonically for $P\geqslant P_{\text{cr}}$, i.e., in the presence of the rippling bending mode.

We now recall the report of Poncharal *et al.*[15] that the modulus they calculated from the classical modulus-frequency relation (1) using the measured resonance frequency was found to decrease sharply from 1 to 0.1 TPa with the diameter increasing from 8 to 40 nm and that a rippling bending mode was observed for nanotubes of larger diameters. According to the above analysis, the modulus Poncharal *et al.*[15] calculated is the effective Young's modulus in the presence of rippling and their work indicates that the effective Young's modulus, instead of the actual Young's modulus, decreased sharply at the emergence of the rippling bending mode and with its subsequent progressive development, and we should credit Poncharal and his colleagues for later referring to their so-calculated modulus as the bending modulus, a point of caution to the readers well exercized. We are much encouraged by this qualitative consistence, but a quantitative comparison of this analysis with their measurements is, however, not possible at this point due to a lack of information required. In their experiment,[15] the harmonic oscillating voltage was adjusted in each test to maximize the vibration for each individual nanotube, and this voltage amplitude was not recorded.[33,34] Furthermore, the lengths of these sample nanotubes were reported only for a very few groups of samples, and we note that measuring the lengths of these nanotubes accurately is not an easy task because they used a fiber composed of carbon nanotubes recovered from the nanotube arc deposit. Nevertheless, to illustrate one of the implications of this analysis that the effective modulus E_{eff} can drop sharply as the rippling bending mode emerges, we plot in Fig. 4 the effective Young's modulus versus the diameter d, using the graphite base Young's modulus $E=1.02$ TPa, for fixed length $L=1$ μm and displacement/length ratio $\Delta_0/L=0.3$. We see that the effective Young's modulus E_{eff} has the same value as the actual Young's modulus E for small diameter and it decreases sharply as the diameter d becomes slightly larger than a critical value $d_{\text{cr}}\approx 12$ nm, corresponding to the emergence of the rippling mode. We note, with caution, that the numerical values for the length and the displacement/length ratio were chosen, by trial and error, to fit the data obtained from the measurements of Poncharal *et al.*[15] for the sole purpose of illustration.

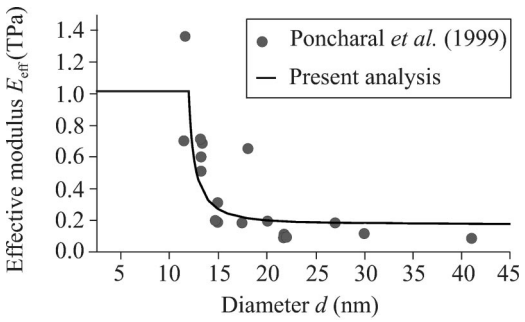

FIG. 4. The effective Young's modulus versus the diameter d. The dots are reproduced from the experimental records by Poncharal *et al.* (Ref. 15) (see their Fig. 4A). The solid line is the model prediction, with the fixed length $L=1$ μm and displacement/length ratio $\Delta_0/L=0.3$ chosen to fit the measured data for the purpose of illustration.

To conclude our discussion, we would like to remark that one needs to be particular cautious in using the classical results from the linear elasticity to derive the mechanical properties of carbon nanotubes from measurements, because their responses to probing are not always linear. The rippling bending mode, observed by several investigators, Ruoff and Lorents,[22] Kuzumaki *et al.*,[23] and Poncharal *et al.*,[15] appears to be responsible for the unusual mechanical behaviors in bending deflection reported by Wong *et al.*[13] and in resonant vibration reported by Poncharal *et al.*[15]

ACKNOWLEDGMENTS

We gratefully acknowledge the support of the Chinese National Science Foundation through the Grants No. 10172051 and No. 10252001, the U.S. National Science Foundation through Grant No. CMS-0140568, the Ministry of Education of China, Tsinghua University, and the University of California at Riverside.

*Email address: zhengqs@tsinghua.edu.cn
†Email address: qjiang@engr.ucr.edu

[1] S. Iijima, Nature (London) **354**, 56 (1991).
[2] D. H. Robertson, D. W. Brenner, and J. W. Mintmire, Phys. Rev. B **45**, 12 592 (1992).
[3] P. Calvert, Nature (London) **357**, 365 (1992).
[4] G. Ovemey, W. Zhong, and D. Z. Tomanek, Phys. Rev. D **27**, 93 (1993).
[5] B. I. Yakobson, C. J. Brabee, and J. Bernhole, Phys. Rev. Lett. **76**, 2511 (1996).

[6] A. Krishnan, E. Dujardin, T. W. Ebbesen, P. N. Yianilos, and M. M. J. Treacy, Phys. Rev. B **58**, 14 013 (1998).
[7] M.-F. Yu, B. S. Files, S. Arepalli, and R. S. Ruoff, Phys. Rev. Lett. **84**, 5552 (2000).
[8] S. Akita, H. Nishijima, Y. Nakayama, F. Tokumasu, and K. Takeyasu, J. Phys. D **32**, 1044 (1999).
[9] J. Cumings and A. Zettl, Science **289**, 602 (2000).
[10] Q.-S. Zheng and Q. Jiang, Phys. Rev. Lett. **88**, 45 503 (2002).
[11] Q.-S. Zheng, J. Z. Liu, and Q. Jiang, Phys. Rev. B **65**, 245409 (2002).
[12] M. M. J. Treacy, T. W. Ebbesen, and J. M. Gibson, Nature (London) **381**, 678 (1996).
[13] E. W. Wong, P. E. Sheehan, and C. M. Liebert, Science **277**, 1971 (1997).
[14] J.-P. Salvetat *et al.*, Adv. Mater. **11**, 161 (1999).
[15] P. Poncharal, Z. L. Wang, D. Ugarte, and W. A. de Heer, Science **283**, 1513 (1999).
[16] L. Meirovich, *Fundamentals of Vibrations* (McGraw-Hill, New York, 2000).
[17] M.-F. Yu, O. Lourie, M. J. Dyer, K. Moloni, T. F. Kelly, and R. S. Ruoff, Science **287**, 637 (2000).
[18] M.-F. Yu, B. S. Files, S. Arepalli, and R. S. Ruoff, Phys. Rev. Lett. **84**, 5552 (2000).
[19] B. I. Yakobson and P. Avouris, Top. Appl. Phys. **80**, 287 (2001).
[20] C. Q. Ru, Phys. Rev. B **62**, 9973 (2000).
[21] J. Z. Liu, Q.-S. Zheng, and Q. Jiang, Phys. Rev. Lett. **86**, 4843 (2001).
[22] R. S. Ruoff and D. C. Lorents, Carbon **33**, 925 (1995).
[23] T. Kuzumaki *et al.*, Philos. Mag. A **77**, 1461 (1998).
[24] S. Iijima, C. Brabec, A. Maiti, and J. Bernholc, J. Chem. Phys. **104**, 2089 (1996).
[25] R. E. Smalley and B. I. Yakobson, Solid State Commun. **107**, 597 (1998).
[26] T. W. Ebbesen, Phys. Today **49**, 26 (1996).
[27] D. H. Robertson and C. T. White, Phys. Today **49**, 5 (1996).
[28] A. Garg and S. B. Sinnott, Phys. Rev. B **60**, 13 786 (1999).
[29] A. G. Every and A. K. McCurdy, in *Numerical Data and Functional Relationships in Science and Technology, Group III: Crystal and Solid State Physics*, edited by D. F. Nelson (Springer-Verlag, Berlin, 1992).
[30] B. T. Kelly, *Physics of Graphite* (Applied Science, London, 1981).
[31] A. J. M. Spencer, *Continuum Mechanics* (Longman, London, 1980).
[32] Our further numerical simulations (J. Z. Liu, Studies on several mechanical problems of carbon nanotubes, Ph.D. thesis, Tsinghua University, 2002 based on a shell-cobweb model, for bending a 40-nm-length, 5-nm-diameter carbon nanotubes show that the rippling mode always emerges at severe bending for nanotubes of 6 or more walls, while for nanotubes of fewer walls, one, two or four kinks, instead of rippling, develop at severe bending. Our analysis and simulations suggest that rippling appears to be associated with the multiplicity of walls of MWNT's and the ultralow interwall sliding resistance strength (ISRS) (Refs. 9–11,17,18). The bilinear relation (3) captures, approximately, the constitutive behavior of multiwalled carbon nanotubes near rippling although the dimensionless parameters $\bar{\kappa}_{cr}$ and α vary with configurations of individual tubes. For instance, we find that the predicted responses of the lateral force and the strain energy versus the deflection fit the measurements of Wong *et al.* (Ref. 13) remarkably well, if we set $\bar{\kappa}_{cr} \approx 0.012$ and $\alpha \approx 0.31$, for a six-walled nanotube of 40-nm in length and 5-nm in diameter, taking the interwall spacing to be 0.34 nm.
[33] P. Poncharal (private communication).
[34] The loading P is applied by controlling the displacement Δ_A of the AFM probe, whose tip is located at the free end of the AFM's cantilevered beam. The relative displacement Δ_{tip} of the probe tip to the controlled displacement Δ_A is recorded and it is proportional to P in the form $\Delta_{tip}=P/k_A$ with the known AFM elastic stiffness parameter k_A. This leads to the deflection $\Delta=\Delta_A-\Delta_{tip}$. When $P<P_{cr}$, or equivalently, $\Delta<\Delta_{cr}$, the classical prediction $\Delta=P/k$ with $k=3EI/L^3$ is valid. As Δ_A is increasingly crossing the critical value Δ_A^{cr} with respect to P_{cr} and Δ_{cr}, the bending mode is transiting from the classical mode to the rippling one. Prior to the emergence of the first rippling period (which is about one fourth of the nanobeam height), the nanobeam becomes kinked at the cantilevered end ($x=0$), with a certain kinked angle denoted by θ_k. Denoting by (P_{cr}^-,Δ_{cr}^-) and (P_{cr}^+,Δ_{cr}^+), respectively, the loading/displacement pairs immediately before and after the kinking and neglecting the dynamic effect, we have

$$\frac{P_{cr}^-}{k}+\frac{P_{cr}^-}{k_A}=\Delta_A^{cr},\quad \frac{P_{cr}^+}{k}+\theta_k L+\frac{P_{cr}^+}{k_A}=\Delta_A^{cr}.$$

It thus yields

$$P_{cr}^+=(\Delta_A^{cr}-\theta_k L)/(1/k+1/k_A)<P_{cr}^-=\Delta_A^{cr}/(1/k+1/k_A),$$

$$\Delta_{cr}^+=\Delta_A^{cr}-P_{cr}^+/k_A>\Delta_{cr}^-=\Delta_A^{cr}-P_{cr}^-/k_A.$$

In other words, as the AFM probe displacement Δ_A increases to exceed Δ_A^{cr}, a kink develops at the fixed end, causing the loading to drop $(P_{cr}^+-P_{cr}^-<0)$ and correspondingly, the displacement to rise $(\Delta_{cr}^+-\Delta_{cr}^->0)$. The normalized slope is

$$\frac{\bar{P}_{cr}^+-P_{cr}^-}{\bar{\Delta}_{cr}^+-\bar{\Delta}_{cr}^-}=\frac{P_{cr}^+-P_{cr}^-}{\Delta_{cr}^+-\Delta_{cr}^-}\frac{\Delta_{cr}}{P_{cr}}=-\frac{k_A}{k}<0.$$

The above result is consistent with the force-displacement measurment of Wong *et al.* (Ref. 13) in their Fig. 4A. For a qualitative comparison, the dotted line in Fig. 2 is plotted having taken into account of the above kinking effect.